Characterizing Inclusions in the Weld Metal of EH36 Shipbuilding Steel Processed by CaF_2-30 Wt Pct TiO_2 Flux

XIAOBO YUAN, MING ZHONG, YONGWU WU, and CONG WANG

EH36 shipbuilding steel has been submerged arc welded by employing CaF_2-30 wt pct TiO_2 flux, and the inclusion characteristics have been documented. After welding, the inclusion number density increases while its size as an ensemble shrinks. It is postulated that TiO_2 in the flux serves as a viable way of promoting the formation of Ti-containing inclusions by incurring Ti and O transfer. Besides, the inclusion distribution is largely dictated by the flow of the weld-pool.

https://doi.org/10.1007/s11663-022-02455-z

EH36 is a typical low-alloy high-strength marine structural steel with remarkable low-temperature toughness and superb weldability.[1] Due to its high deposition rate and excellent weld quality, submerged arc welding (SAW) has been widely applied as a major technology for shipbuilding, pipeline, and offshore platform manufacturing, which can greatly improve production efficiency and significantly shorten building time.[2,3] For the submerged arc welded products, end-user material properties are largely dictated by the weld metal (WM).[4]

Formation of nonmetallic inclusions in the WM is inevitable during the SAW process, and the inclusions' roles as initiation sites for acicular ferrites (AFs) are widely accepted.[5,6] WM inclusions are natural products involving complex physical and chemical reactions under the interactions among the molten weld pool, welding flux, and arc plasma.[7] Therefore, crucial factors pertinent to inclusions, such as morphology, composition, number density, and size distribution, are deemed to play decisive roles in optimizing the final WM microstructure.[8]

It has been suggested that the compositions of the employed fluxes are important, as they constitute the major sources of O and other alloying elements.[7,9] Application of different types of fluxes with various oxide components, such as TiO_2, SiO_2, and MnO, presents a major feasible means to generate corresponding categories of oxide inclusions.[10,11] TiO_2, which can improve arc stability, reduce slag viscosity, and release O during SAW, is often adopted for designing the CaF_2-type fluxes.[12–15] Zhang *et al.*[16] revealed that the change of TiO_2 content in basic-fluoride-type agglomerated commercial fluxes imposed a remarkable effect on the inclusion size distribution in the WM but failed to distinguish the variations of inclusion characteristics from the base metal (BM), such as the type, the formation mechanism, and their effect on microstructure. Moreover, studies have shown that the distribution of inclusions has a great influence on the microstructure of the WM.[2,5,16] However, due to the complex nature of fluxes and the complicated welding thermal process, convincing spatial distribution of inclusions in the WM has not been described. The current study aims to profile variations of inclusion morphology, composition, number density, and size distribution in EH36 shipbuilding steel after SAW by using the TiO_2-bearing flux. The spatial distribution characteristics of inclusions across the entire WM will be revealed in detail, and their potential impact upon WM microstructures will be elaborated.

CaF_2-30 wt pct TiO_2 fused flux was prepared, as such composition coincided well with the eutectic point, potentially allowing sufficient alloying element transfer and improved slag detachability.[14,17,18] Totally, 700 g of CaF_2 (> 98.5 mass pct) and 300 g of TiO_2 (> 99.0 mass pct) reagent powders were weighed as raw materials, and these powders were mixed 30 minutes in a V blender (DELIXI, China). Afterward, mixed powders were placed in a graphite crucible and were melted for 1 hour at 1823 K (1550 °C) in an induction furnace, during which the crucible was sealed to minimize the evaporation of fluoride species.[19] Subsequently, the melting flux was quenched by cold water. The solidified flux particles were dried, crushed, and sieved into 12 to 200 mesh, and then baked at 973 K (700 °C) for 2 hours to remove residual graphite and moisture. Chemical compositions of the flux were determined by X-ray

XIAOBO YUAN, MING ZHONG, YONGWU WU, and CONG WANG are with the School of Metallurgy, Northeastern University, Shenyang 110819, China. Contact email: wangc@smm.neu.edu.cn
Manuscript submitted November 29, 2021; accepted January 20, 2022. Article published online February 14, 2022.

fluorescence spectroscopy (XRF, model S4 Explorer). Differences between designed and analytical CaF_2 and TiO_2 were within 5 pct and are deemed as negligible.[20]

EH36 shipbuilding steel with a thickness of 24 mm was used as the BM. Single-pass bead-on-plate SAW was performed using a double-wire welding machine (Lincoln Electric Power Wave AC/DC 1000 SD, Lincoln Electric, China). The welding speed was set as 500 mm/min, and a 60 kJ/cm heat input (DC-850 A/32 V for welding wire forward, and AC-625 A/36 V for welding wire backward) was employed. Metallic elements were analyzed by an inductively coupled plasma optical emission spectrometer (ICP-OES, 8300 DV, Perkin Elmer Optima), and C and O were analyzed using a LECO* analyzer (CS230 for C and ONH836 for O). Compositions of the welding wire, BM, and WM are summarized in Table I.

*LECO is a trademark of LECO Corporation, St. Joseph, MI.

WM samples were cut along the cross section perpendicular to the welding direction. Three samples of the WM from the perpendicular central axis marked as middle (middle position of the WM, named WM-M), top (4.5 mm upward from the middle position of the WM, WM-T), and bottom (4.5 mm downward from the middle position of the WM, WM-B) were obtained, as shown in Figure 1. Subsequently, the samples were mechanically ground, polished, and etched by 4 wt pct nitric acid solution. The morphology and corresponding chemical compositions of typical inclusions were observed and determined by scanning electron microscope (SEM, MAIA3XMH, TESCAN, CZ (Brno, Czech Republic)) with an energy dispersive spectrometer (EDS) at 20 kV acceleration voltage and 15 mm working distance. Meanwhile, the size and quantity of inclusions were identified at a magnification of 5000 times, and at least 100 fields of view (0.5 mm × 0.5 mm) were examined for each position.

The sample used for inclusion examination of the WM was from WM-M, as this position is the most representative one.[21] Figure 2 shows the typical morphologies and compositions of inclusions in the BM and WM-M. The shapes of the predominating inclusions in the BM can be classified as polygonal (Figures 2(a) and (b)) and irregular (Figures 2(c)) according to the typical appearance. The inclusions in WM-M are largely spherical (Figures 2(d) and (e)) and cuboidal (Figure 2(f)) in morphology.

Table I. Chemical Compositions of Welding Wire, BM, and WM (Weight Percent)

Composition	C	Mn	Si	Ni	Ti	O
Welding wire	0.127	1.650	0.049	0.009	0.010	0.003
Base metal	0.052	1.540	0.142	0.075	0.010	0.003
Weld metal	0.071	1.090	0.072	0.046	0.041	0.017

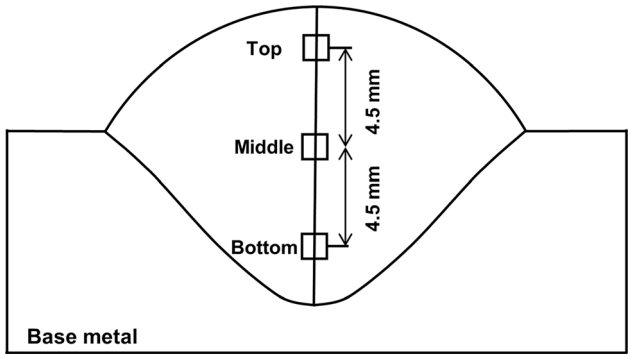

Fig. 1—Sampling regions for inclusion examinations.

Inclusion compositions were analyzed by EDS and the results are expressed in atomic percentages. Typical inclusions in the BM are O-Al-Mg-Si-(Ti)-Mn-S complex categories and single-phase MnS particles, as shown in Figures 2(a) through (c). However, in WM-M, the majority of inclusions are dominantly Ti-rich oxide types. Single-phase inclusions appear to be composed of O-Al-Ti-(Si)-(Mn) oxide (Figures 2(d) and (e)), while multiphase inclusion features a spherical O-Al-Ti-(Si)-(Mn) oxide core and a TiN shell, as shown in Figure 2(f). Ilman *et al.*[22] reported that the thin outer layer formed on the Al_2O_3 and TiO_X inclusion surface was likely to be TiO or TiN phase.

Zhang *et al.*[12] documented a model based on the thermodynamic gas-slag-metal equilibrium to illustrate the impact of TiO_2 on the transfer behaviors of Ti and O when a series of TiO_2-bearing basic-fluoride fluxes were applied. Owing to the high temperature and surface-to-volume ratio, a local momentary equilibrium is available in the hot zone of the weld pool and the slag-metal reaction could take place.[18,21] Mitra and Eagar[18] and Zhang *et al.*[13,16] reported that Ti was transferred from the slag to the weld pool at the slag-metal interface *via* Reaction [1]. In addition, as shown in Table I, Ti and O contents in the BM and the welding wire are much lower than those in the WM. Therefore, the major source of O is considered to be from the TiO_2 ingredient *via* flux decomposition or flux entrapment under the arc plasma.[12] It is expected that the reaction products exist as inclusions in the WMs, and the transferred Ti and O provide a favorable chemical condition for the formation of Ti-containing inclusions in SAW.

$$(TiO_2) = [Ti] + 2[O] \quad [1]$$

Inclusions with special chemical compositions and structures are able to trigger the nucleation of AF, which is essential for the development of the fine microstructure in the WM.[5,22] Figure 3 shows a typical SEM micrograph of WM-M demonstrating nucleated AFs surrounding a typical inclusion, of which elemental mappings suggest the nature of the inclusion being TiO_X-Al_2O_3-MnO as the core and TiN as the outer layer. It is reported that the structure of multilayer inclusions varies from the core to the surface, indicating that high melting point oxides were initially formed as

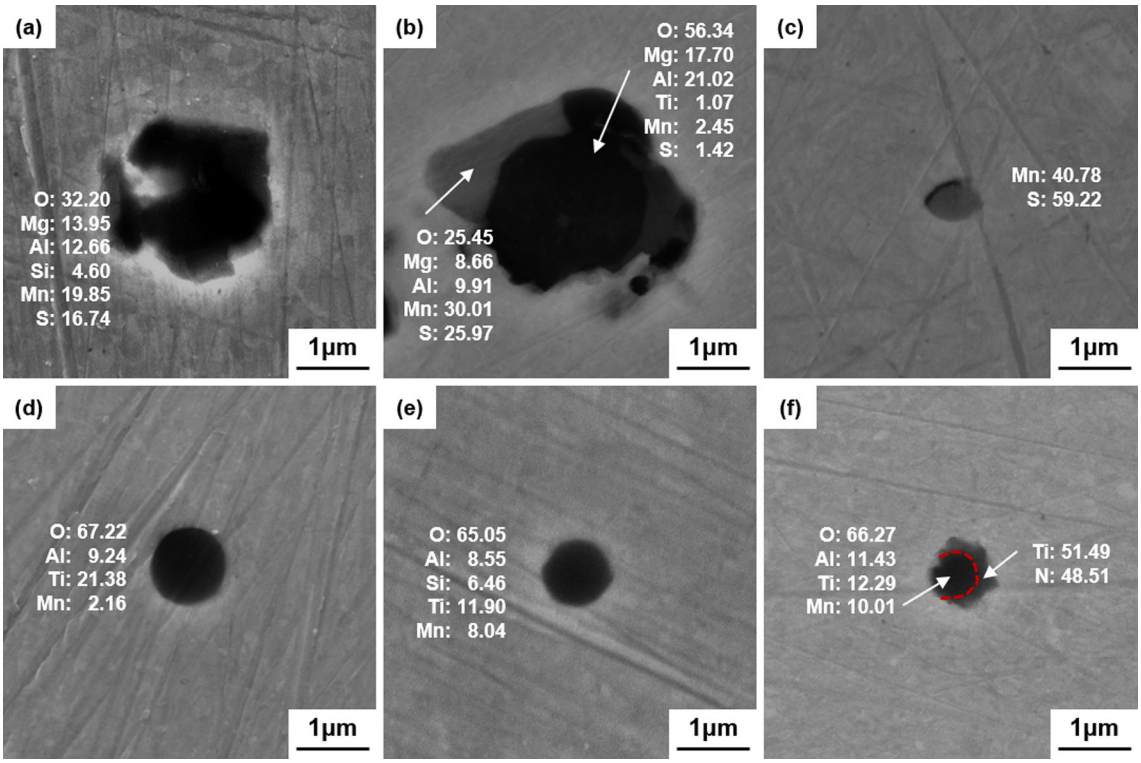

Fig. 2—Morphologies and compositions of inclusions in (*a*) through (*c*) the BM and (*d*) through (*f*) WM-M.

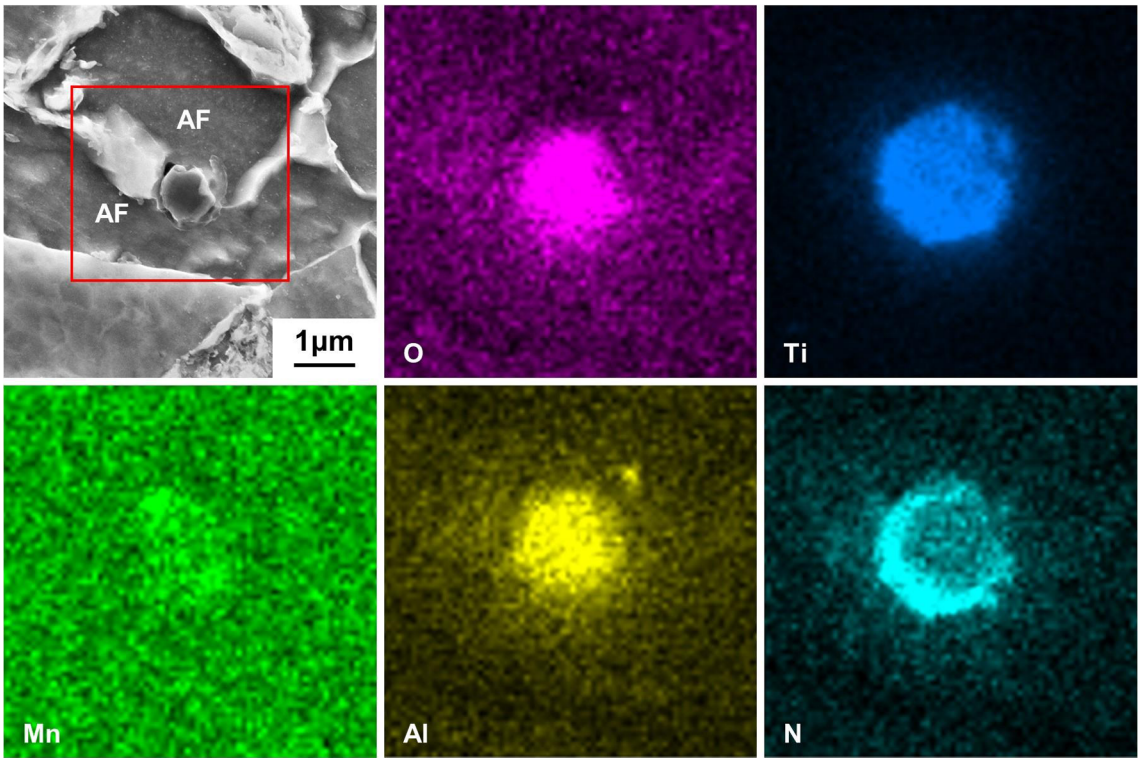

Fig. 3—SEM micrograph and elemental mappings of a typical complex inclusion nucleating AF in WM-M.

the nuclei.[7,23] Subsequently, during the solidification process, alloying elements, such as Ti, Mn, N, and S, in the liquid metal may gradually diffuse to the vicinity of the crystal nucleus; then, the TiN and MnS phases precipitate and adhere to the previously formed core as an inclusion surface coating.[23–25] In addition, it is

evident that the two AFs grow radially centered on the inclusion, nucleating at the junction between TiN and Ti-Al-Mn oxide core or on the surface of TiN shell. The "Mn depletion zone" mechanism may be one of the important interpretations for AF nucleation.[5] Also, the low lattice mismatch between the TiN phase and ferrite matrix (about 4.7 pct) enhances the driving force for AF nucleation by reducing the nucleation energy barrier.[23,26]

Figure 4 shows the statistics of inclusion number density with different sizes in the BM and WM-M. The inclusion numbers in each field were counted and the sizes of inclusions (d_i) were measured using ImageJ software. The d_i was estimated as a circle diameter having the same cross-sectional area of the observed inclusion. The number density of inclusions for the per unit area (N_A) was calculated according to Eq. [2]:

$$N_{\mathrm{A}} = N_{\mathrm{obs}}/A_{\mathrm{obs}} \qquad [2]$$

where A_{obs} is the total observed area and N_{obs} is the number of inclusions in the given observed area.

The total inclusion number density is about 344 N/mm^2 in the BM. The sizes of individual MnS and nitrides mainly fall in the range between 0.1 and 1 μm, as shown in Figure 4(a), which is consistent with the results of Wang *et al.*[27] Besides, oxide inclusions are mainly distributed from 0.5 to 5 μm with a number density of around 244 N/mm^2. After SAW, typical Ti-containing inclusions are mainly distributed at the nanoscale, and a sizable amount of WM inclusions are smaller compared with those from the BM. In addition, since nearly all O exists as oxides due to the low solubility of O in the steel matrix, the inclusion number density is mainly governed by the O content.[6,8,28] A sharply enhanced O content in the WM promotes a significant increase in the inclusion number density after welding so that the number of inclusions increases to about 5670 N/mm^2 in WM-M, as shown in Figure 4(b). Furthermore, it should be noted that MnS is not stable at high temperature (around 1473 K), and the formation of individual MnS is prevented due to the changed solubilities of Mn and S during welding.[1,29] Hence, almost no individual MnS inclusions are formed after SAW.

For the steelmaking process, the buoyancy effect plays a role in removing the deoxidation products from the molten pool; that is, the rising velocity of an inclusion (v) relative to the liquid follows Stokes' law presented in Eq. [3]:[30]

$$v = (gd_i^2\Delta v\rho)/(18\eta) \qquad [3]$$

where g is the gravitational constant, d_i is the diameter of the inclusion, $\Delta\rho$ is the difference in densities between liquid steel and inclusions, and η is the viscosity of liquid steel. The holding time of deoxidation is usually limited to less than 20 minutes, which allows the particles larger than 200 μm to float, while the inclusions smaller than 10 μm would be entrapped even after the refining stage.[31] It is noted that the growth of inclusions is relatively slow, requiring sufficient time to allow the atomic nuclei to grow into particles with several microns through the solute diffusion or even further collision.[31] In recorded experiments, the maximum inclusion size increases rapidly after holding for 30 seconds and the average size of inclusions increases with the holding time.[32] However, for the welding process, the formation and growth of inclusions are often completed within a few seconds such that the growth of a majority inclusion is retarded due to the high cooling rate.[33] Furthermore, due to inadequate stirring in the "cold" zone of the weld pool, the possibility of collision and coalescence behavior is reduced.[8,30] Therefore, it is expected that the WM inclusions with small sizes might result from the large cooling rate and insufficient stirring during the solidification process. In addition, the rising velocity of the inclusions smaller than 1 μm is about five

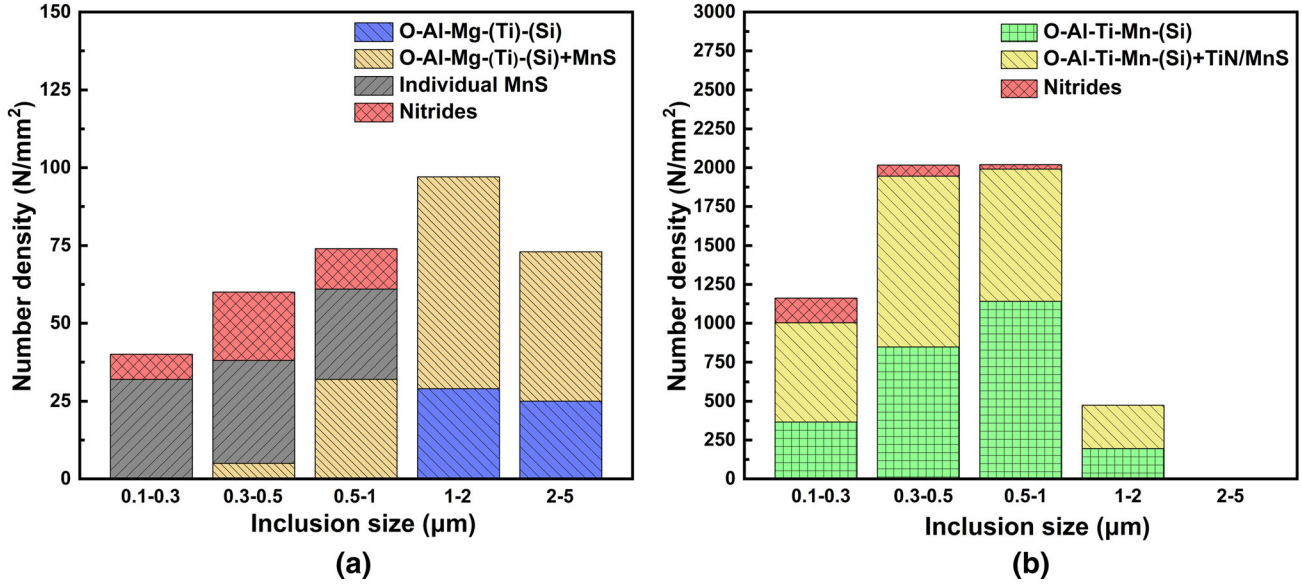

Fig. 4—Number density and size distribution of inclusions in (*a*) the BM and (*b*) WM-M.

orders of magnitude lower than those in the liquid steel during deoxidation.[30] Consequently, the rising velocity of these WM inclusions is far from satisfying the Stokes' law so that the floatation caused by buoyancy can be ignored.

Figure 5 shows the distribution of inclusions at different locations across the WM. Generally, under the effect of fluid flow, the distribution of inclusions in the WM is not uniform at comparable spatial dimensions.[34,35] The results show that no matter where the inclusions are located in the WM, the size distribution of inclusions follows the log-normal pattern. It shows that the number density of inclusions gradually increases from 3736 N/mm^2 (WM-T) to 5670 N/mm^2 (WM-M) and 7212 N/mm^2 (WM-B), with the average size decreasing from 0.58 μm (WM-T) to 0.47 μm (WM-M) and 0.35 μm (WM-B), respectively. The frequency peaks of the inclusion size at WM-T, WM-M, and WM-B are 0.4 to 0.5 μm, 0.3 to 0.4 μm, and 0.2 to 0.3 μm, respectively. It is found that when the inclusions are located in WM-T, the number of inclusions decreases, especially for those smaller than 0.3 μm in size. In addition, the inclusions in WM-T are concentrated in the range of 0.3 to 0.7 μm, while in WM-B, they are mainly distributed in the range of 0.1 to 0.4 μm.

Hong *et al.*[34] calculated the thermal history, growth, and dissolution behavior of inclusions, showing that most inclusions experience spatial motion and thermal excursions; that is, inclusions dwelling in the weld pool would undergo dissolution, regrowth, and collision.[36] During continuous cooling, inclusions are more likely to nucleate in the region with a small fluid flow velocity, *i.e.*, near the boundary between the fusion zone and heat affected zone. Also, the temperature in this region is lower, and the melt stirring, to a great extent, does not take place.[30,34,35] As a result, more tiny inclusions are trapped in WM-B. However, at higher temperatures, due to the prevailing fluid flow and a certain degree of stirring action, inclusions with relatively small size will be dissolved; meanwhile, the chance of regrowth and collision of partial inclusions may be increased under the same conditions, facilitating the rise of larger inclusions to ascend to WM-T.[30] Therefore, fluid flow transports inclusions to different temperature regions and controls the separation and flotation of inclusions. Thus, it is feasible that the fluid flow determines the spatial distribution of inclusions across the WM.

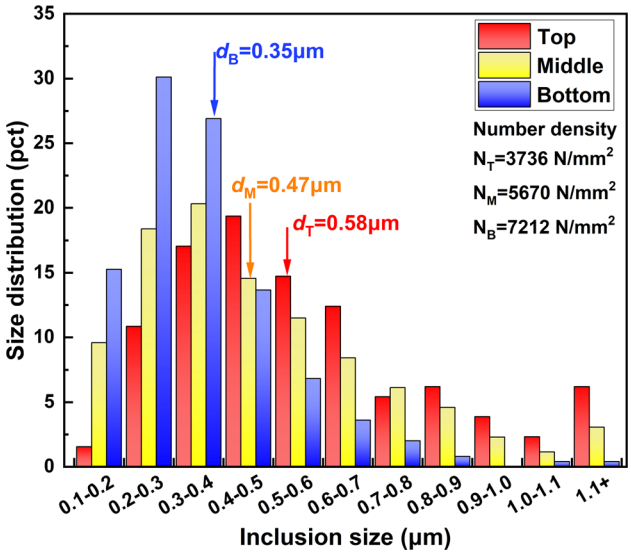

Fig. 5—Number density and size distribution of inclusions at different WM locations. N_T, N_M, and N_B represent the inclusion number density at WM-T, WM-M, and WM-B, respectively; d_T, d_M, and d_B represent the inclusion average size at WM-T, WM-M, and WM-B, respectively.

In summary, EH36 shipbuilding steel has been processed by applying CaF_2-30 wt pct TiO_2 flux under SAW, and ensued WM inclusions have been characterized with regard to chemical composition, number density, and size distribution. The main results are summarized as follows:

1. TiO_2 in the welding flux serves as a viable way of altering WM chemistry by incurring Ti and O transfer and promoting the formation of single-phase Al-Ti-(Si)-(Mn)-O inclusions and multiphase inclusions composed of Al-Ti-(Si)-(Mn)-O complex oxide core and TiN shell. In addition, AFs are found to nucleate on the surface of Ti-containing inclusions.
2. After SAW, the total number density of inclusions sharply increases from 344 to 5670 N/mm^2 (WM-M), while the size shrinks remarkably. The size of inclusions is mainly concentrated in the range of 0.1 to 2 μm, and inclusions show log-normal distribution patterns across the WM. Compared with WM-M, the number of inclusions at WM-B is significantly reduced, with an average size of 0.35 μm, while inclusions located at WM-T are less but larger due to the fluid flow.

ACKNOWLEDGMENTS

The authors sincerely thank the National Natural Science Foundation of China (Grant Nos. U20A20277, 51861145312, 52011530180, and 52050410341), Royal Academy of Engineering (TSPC1070), Research Fund for Central Universities (Grant Nos. N2125003, N2125016, and N2025025), Regional Innovation Joint Fund of Liaoning Province (2020-YKLH-39), Key Laboratory for Ferrous Metallurgy and Resources Utilization of Ministry of Education, Wuhan University of Science and Technology (FMRUlab-20-5), Open Project of State Key Laboratory of Advanced Special Steel, Shanghai Key Laboratory of Advanced Ferrometallurgy, Shanghai University (SKLASS 2020-09) and the Science and Technology Commission of Shanghai Municipality (No. 19DZ2270200).

CONFLICT OF INTEREST

On behalf of all authors, the corresponding author states that there is no conflict of interest.

REFERENCES

1. X. Zou, J. Sun, D. Zhao, H. Matsuura, and C. Wang: *J. Iron Steel Res. Int*., 2018, vol. 25, pp. 164–72.
2. N. Yan, S.F. Yu, and Y. Chen: *Sci. Technol. Weld. Join*., 2015, vol. 20, pp. 418–24.
3. C. Wang and J. Zhang: *Acta Metall. Sin*., 2021, vol. 57, pp. 1126–40.
4. K. Sirin, S.Y. Sirin, and E. Kaluc: *Int. J. Adv. Manuf. Technol*., 2016, vol. 87, pp. 1941–50.
5. Y. Kang, S. Jeong, J.H. Kang, and C. Lee: *Metall. Mater. Trans. A*., 2016, vol. 47A, pp. 2842–54.
6. Y. Kang, J. Jang, J.H. Park, and C. Lee: *Metall. Mater. Int*., 2014, vol. 20, pp. 119–27.
7. S.A. Court and G. Pollard: *Metallography*., 1989, vol. 22, pp. 219–43.
8. D.R. Eo, S.H. Park, and J.W. Cho: *Mater. Des*., 2018, vol. 155, pp. 212–19.
9. B.R. Keville: *Weld. J*., 1983, vol. 62, pp. 253–60.
10. F. Khamouli, M. Zidani, K. Digheche, A. Saoudi, and L. Atoui: *Diffus. Found*., 2018, vol. 18, pp. 55–64.
11. F. Khamouli, M. Zidani, H. Farh, A. Saoudi, and L. Atoui: *Int. J. Eng. Res. Afr*., 2016, vol. 27, pp. 11–19.
12. J. Zhang, T. Coetsee, S. Basu, and C. Wang: *Calphad*, 2020, vol. 71, p. 102195.
13. J. Zhang, T. Coetsee, H.B. Dong, and C. Wang: *Metall. Mater. Trans. B*., 2020, vol. 51B, pp. 1953–57.
14. C. Natalie, D. Olson, and M. Blander: *Annu. Rev. Mater. Sci*., 1986, vol. 16, pp. 389–413.
15. Y.Y. Zhang, T. Coetsee, H.F. Yang, T. Zhao, and C. Wang: *Metall. Mater. Trans. B*., 2020, vol. 51B, pp. 1947–52.
16. J. Zhang, J. Leng, and C. Wang: *Metall. Mater. Trans. B*., 2019, vol. 50B, pp. 2083–87.
17. M. Allibert, H. Gaye, J. Geiseler, D. Janke, B.J. Keene, D. Kirner, M. Kowalski, J. Lehmann, K.C. Mills, and D. Neuschütz: *Slag Atlas*, 2nd ed. Verlag Stahleisen GmbH, Düsseldorf, Germany, 1995, p. 190.
18. U. Mitra and T.W. Eagar: *Metall. Trans. B*., 1991, vol. 22B, pp. 73–81.
19. C.B. Dallam, S. Liu, and D.L. Olson: *Weld. J*., 1985, vol. 64, pp. 140–51.
20. J. Zhang, T. Coetsee, and C. Wang: *Metall. Mater. Trans. B*., 2019, vol. 51B, pp. 16–21.
21. J.E. Indacochea, M. Blander, N. Christensen, and D.L. Olson: *Metall. Trans. B*., 1985, vol. 16B, pp. 237–45.
22. M.N. Ilman, R.C. Cochrane, and G.M. Evans: *Weld. World*., 2015, vol. 59, pp. 565–75.
23. Ø. Grong, A.O. Kluken, H.K. Nylund, A.L. Dons, and J. Hjelen: *Metall. Mater. Trans. A*., 1995, vol. 26A, pp. 525–34.
24. S.S. Babu, S.A. David, J.M. Vitek, K. Mundra, and T. DebRoy: *Mater. Sci. Technol*., 2013, vol. 11, pp. 186–99.
25. M. Li, H. Matsuura, and F. Tsukihashi: *Metall. Mater. Trans. B*., 2019, vol. 50B, pp. 748–60.
26. H.H. Jin, J.H. Shim, Y.W. Cho, and H.C. Lee: *ISIJ Int*., 2003, vol. 43, pp. 1111–13.
27. Q. Wang, X. Zou, H. Matsuura, and C. Wang: *Metall. Mater. Trans. B*., 2017, vol. 48B, pp. 18–22.
28. H. Goto, K. Miyazawa, and K. Tanaka: *ISIJ Int*., 1995, vol. 35, pp. 286–91.
29. X. Zou, H. Matsuura, and C. Wang: *Metall. Mater. Trans. B*., 2019, vol. 50B, pp. 1134–38.
30. Ø. Grong, T.A. Siewert, G.P. Martins, and D.L. Olson: *Metall. Mater. Trans. A*., 1986, vol. 17A, pp. 1797–1807.
31. S. Liu and D.L. Olson: *J. Mater. Eng*., 1987, vol. 9, pp. 237–51.
32. S.S. Babu, S.A. David, and T. DebRoy: *Sci. Technol. Weld. Join*., 1996, vol. 1, pp. 17–27.
33. S.S. Babu and S.A. David: *ISIJ Int*., 2002, vol. 42, pp. 1344–53.
34. T. Hong, T. Debroy, S.S. Babu, and S.A. David: *Metall. Mater. Trans. B*., 2000, vol. 31B, pp. 161–69.
35. A. Yadav, A. Ghosh, and A. Kumar: *J. Mater. Process. Technol*., 2017, vol. 248, pp. 262–74.
36. S.S. Babu, S.A. David, T. Hong, and T. DebRoy: *Off. Scient. Techn. Infor. Techn. Rep*., 1998, pp. 1–8.